JOURNAL OF THEORETICAL AND APPLIED MECHANICS
63, 1, pp. 91-101, Warsaw 2025
https://doi.org/10.15632/jtam-pl/195840

IMPROVED SHERWOOD-FROST PHENOMENOLOGICAL CONSTITUTIVE MODEL SUITABLE FOR POLYMETHACRYLIMIDE FOAM UNDER UNIAXIAL COMPRESSION

Qianying Cen, Ling Liu

School of Aerospace Engineering and Applied Mechanics, Tongji University, Shanghai, China

corresponding author Ling Liu, e-mail: lingliu@tongji.edu.cn

To investigate the stress-strain response of a polymethacrylimide (PMI) foam under uniaxial compression, an improved phenomenological constitutive model based on the Sherwood--Frost model is fitted from the compressive stress-strain curves of the PMI foam. Firstly, new function terms are proposed to describe the effects of temperature, density and strain-rate. Then, the model parameters are determined. Finally, compression experiments and numerical simulation are conducted on PMI foams at different temperatures, densities and strain-rates to verify the modified model. The results show that it can successfully predict the compressive mechanical response of the PMI foam if the effects of density, temperature and strain-rate are considered.

Keywords: polymethacrylimide (PMI) foam, constitutive model, modified Sherwood-Frost model

1. Introduction

Inspired by natural structures, such as hornbill beak, bird wing trabecular bone and balsa wood, lightweight sandwich structures with foams or honeycomb cores have emerged to meet the urgent demand for structural lightness and multifunctionality in engineering fields, which is of great significance for structural lightweight (Hedayati and Sadighi, 2018). Among many foams that can be selected as cores and simultaneously have the similar density, the polymethacrylimide (PMI) foam shows advantages in mechanical properties (such as high specific strength/modulus) and microstructure (rigid closed cell and isotropy) (Palamidi, 2010; Poxon, 2012). Meanwhile, compared with honeycomb, the PMI foam also exhibits excellent secondary processing performance, high interface bonding strength, and the ability to bear side pressure, which enables the PMI foam to support complex profiles and ensures the molding quality of sandwich structures (Maier *et al.*, 2006). In addition, the closed-cell structure of the PMI foam can avoid moisture absorption, which can reduce maintenance expenditure costs. Therefore, the PMI foam is widely used in sandwich structures of helicopter blades, aircraft pressure bulkheads, and rocket vehicles (Seibert, 2006).

In fact, the molding and service of PMI sandwich structures are usually affected by complex working conditions such as temperature and pressure. So, it is particularly important to understand mechanical properties and load-bearing behavior. Li *et al.* (2000) obtained the uniaxial tensile, compressive, pure shear, hydrostatic compressive, and shear-compression properties of PMI foams by experimental tests. Palamidi (2010) investigated the dynamic properties of PMI foams (Rohacell-51WF and 110WF) by using the split Hopkinson pressure bar (SHPB) and direct-impact (DI). Poxon (2012) conducted a comprehensive experimental study on PMI foams with different densities, temperatures and strain rates. Chai *et al.* (2020) performed quasi-static compression of 3D closed-cell PMI foams by in-situ X-ray micro computed tomography (μ-CT).

Huo *et al.* (2022) carried out systematic experimental characterization for elastic, plastic and fracture properties of PMI foams under quasi-biaxial stress loading conditions, and the yield surfaces of PMI foams were calibrated and analyzed. The afore-mentioned studies also show that the compression stress-strain curve of the PMI foam can be divided into three sections, linear elastic section, plateau section, and densification section, and the elastic modulus and plateau section stress increase with the rise of the strain rate and density, but the trend of temperature effect is opposite.

Despite the extensive work that has been done on PMI foams, there are relatively few studies on the constitutive model, because the complexity of the microstructure leads to numerous and complex control parameters of the theoretical model, which is difficult to implement in engineering practice (Li *et al.*, 2022). However, the PMI foam can be assumed as a macroscopic continuum when the size of foam is larger than the typical length of 6 cell bodies (Poxon, 2012), and its stress-strain relationship (including 3 sections) can be easily obtained by a phenomenological method, i.e., achieving a simple parameter identification by fitting experimental data (Sherwood and Frost, 1992). Rusch (1969) established the compression stress-strain function of the polyurethane (PU) foam, and proposed for the first time to use a dimensionless strain function to describe the shape of the compression curve, which was changed into a strain polynomial function by Meinecke and Schwaber (1970) and named the "shape function". Then, Sherwood and Frost (1992) developed a model to decouple the effects of density, temperature, and strain rate on stress, in order to predict the impact response of the PU foam under uniaxial compression. However, previous studies have mainly focused on other polymer foams, such as PU foams, while relatively little research has been done on PMI foams. Meanwhile, there are few studies on the constitutive model of the PMI foam, and often only a single variable was considered, such as density or temperature. Until now, a complete constitutive model that can describe the compressive mechanical behavior of the PMI foam simultaneously considering density, temperature and strain rate has not been publicly reported.

Therefore, the present work aims to investigate the compressive mechanical behavior of the PMI foam under different densities, temperatures and strain-rates. Based on the traditional Sherwood-Frost constitutive model, combined with the experimental data of the PMI foam, an improved model for the PMI foam is proposed, which contains new function terms of temperature, density, and strain rate, as well as the parameters of the new model are determined by fitting the compressive stress-stain curves of the PMI foam. Moreover, the improved model is compared with the model from the previous studies. Finally, compressive experiments and numerical simulation are conducted on PMI foams at different temperatures, densities and strain-rates to verify the improved model.

2. Sherwood-Frost model with modified function terms

In the Sherwood-Frost model, a decoupling function is used to describe the effects of temperature, density and strain rate on the uniaxial compressive stress-strain response of the PU foam (Sherwood and Frost, 1992). In this paper, the general form of this model is employed to predict the mechanical response of the PMI foam under uniaxial compression, as shown in

$$\sigma = H(T)G(\rho)M(\dot{\varepsilon})f(\varepsilon) \tag{2.1}$$

where σ [MPa], T [°C], ρ [kg/m^3], ε and $\dot{\varepsilon}$ [s^{-1}] represent stress, temperature, foam density, strain and strain rate, respectively. Meanwhile, in (Sherwood and Frost, 1992), $H(T)$, $G(\rho)$, $M(\dot{\varepsilon})$ and $f(\varepsilon)$, respectively, denote the bilinear temperature softening term, bilinear density term, exponential strain-rate hardening term, and shape function term which is expressed as a polynomial function

$$f(\varepsilon) = \sum_{i=0}^{n} A_i \varepsilon^i \tag{2.2}$$

where n and A_i represent the order of $f(\varepsilon)$ and the corresponding coefficients of each order, respectively.

On the basis of applying Eq. (2.2) to fit the compressive stress-strain curves of the PMI foam under the reference condition $(\rho_0, T_0, \dot{\varepsilon}_0)$ (Poxon, 2012), the bilinear temperature term $H(T)$ can be further improved into a new negative exponential function of strain, as seen in

$$H(T) = 1 + \frac{1-T}{T_0}\Big[c + b\exp\Big(-\frac{\varepsilon}{a}\Big)\Big] \tag{2.3}$$

where a, b and c are all material parameters, which can be found by approximating the experimental stress-strain data for several temperatures.

Similarly, the density function $G(\rho)$ is proposed to reflect the effect of foam density, which is initially a linear function of relative density $\rho^* = \rho/\rho_0$, as shown in Eq. (2.4) (Sherwood and Frost, 1992)

$$G(\rho) = B(\rho^* - 1) + 1 \tag{2.4}$$

This model only has one parameter B.

Subsequently, considering the influence of foam density on stress is also related to strain, $G(\rho)$ can also be expressed by a modified Freundlich model (Rahimidehgolan and Altenhof, 2023)

$$G(\rho, \varepsilon) = C(\rho) - D(\rho)\varepsilon^{F(\rho)} \tag{2.5}$$

This model has three parameters. The parameters C, D and F are all density dependent.

Because Eqs. (2.4) and (2.5) are suboptimal for the PMI foam, a new density function shown in Eq. (2.6) is constructed by fitting the compression stress-strain curves of the PMI foam in the reference (Poxon, 2012

$$G(\rho^*, \varepsilon) = 1 + (\rho^* - 1)\Big[P(\rho^*) + Q(\rho^*)\exp\Big(\frac{\varepsilon}{R(\rho^*)}\Big)\Big] \tag{2.6}$$

which is an exponential function of relative density, where P, Q and R are all material parameters and related to relative density.

Besides, the strain-rate function $M(\dot{\varepsilon})$ mainly considers the influence of strain-rate, which can be calculated by using the Seeger model (Hu *et al.*, 1998), as shown as

$$M(\dot{\varepsilon}) = 1 + K \lg \frac{\dot{\varepsilon}}{\dot{\varepsilon}_0} \tag{2.7}$$

The parameters K in this model can be fitted by experimental stress-strain data for several strain rates.

Because the influence of strain-rate on stress is also related to strain, thus the strain is coupled with the strain-rate, and so K in Eq. (2.7) is no longer a constant, which can be rewritten as (Jeong *et al.*, 2012)

$$M(\varepsilon, \dot{\varepsilon}) = 1 + (p + q\varepsilon)\ln \frac{\dot{\varepsilon}}{\dot{\varepsilon}_0} \tag{2.8}$$

There are two parameters, p and q, in this model, which can be determined by data fitting.

In fact, Eq. (2.8) is also not well applicable to the PMI foam, so an improved strain-rate function is constructed by fitting the compression stress-strain curves in references (Poxon, 2012) and (Flores-Johnson *et al.*, 2008), as seen as

$$M(\varepsilon, \dot{\varepsilon}) = 1 + (i + j\varepsilon^k)\ln \frac{\dot{\varepsilon}}{\dot{\varepsilon}_0} \tag{2.9}$$

where i, j and k are all strain rate dependent parameters.

3. Determination of constitutive model parameters and verification

3.1. Constitutive model parameters

3.1.1. Determination of shape function parameters

Here, $\rho_0 = 51\,\mathrm{kg/m^3}$, $T_0 = 20°\mathrm{C}$ and $\dot{\varepsilon}_0 = 0.01\,\mathrm{s^{-1}}$ are chosen as the reference condition. As shown in Fig. 1a, a polynomial fitting is used for the compressive stress-strain curve of the PMI foam (Rohacell 51WF) obtained from reference (Poxon, 2012). In order to fit more accurately, the least square method is used to fit a 9-order polynomial, i.e., the shape function $f(\varepsilon)$ of Eq. (2.2) ($n = 9$). The fitted curve and model parameters are respectively given in Figs. 1a and 1b, with a R-Square (R^2) of 0.998. Also, the fitting curve in Fig. 1a indicates that by selecting a 9th-order polynomial as the shape function $f(\varepsilon)$ a very good fitting result can be obtained.

(a)

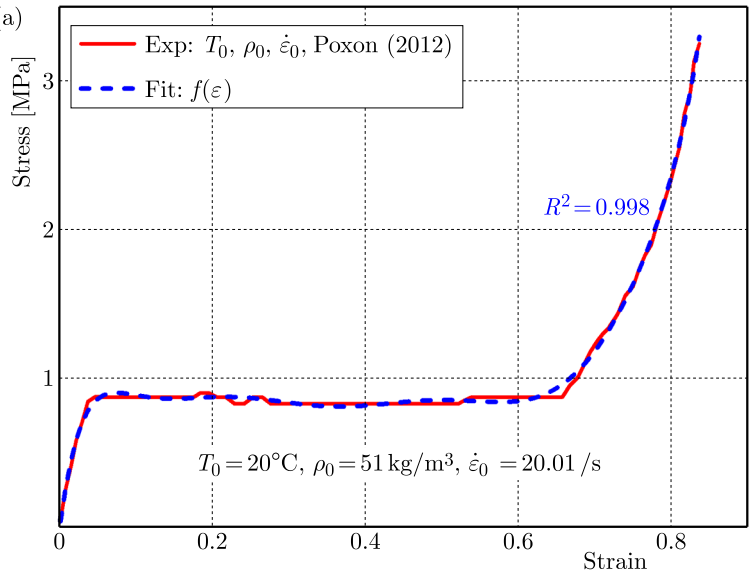

(b)

A_0	A_1
-0.046	41.18
A_2	A_3
-689.91	5917.08
A_4	A_5
-29184.90	87122.53
A_6	A_7
-159554.92	174922.70
A_8	A_9
-105231.16	267707.07

Fig. 1. (a) Fitting curve for the shape function $f(\varepsilon)$ and (b) the obtained model parameters of $f(\varepsilon)$

3.1.2. Determination of temperature function parameters

The compressive stress-strain response of the PMI foam is sensitive to temperature. Keeping the density $\rho_0 = 51\,\mathrm{kg/m^3}$ and strain-rate $\dot{\varepsilon}_0 = 0.01\,\mathrm{s^{-1}}$ unchanged, the compressive stress-strain curves (Rohacell 51WF) at $-70°\mathrm{C}$, $-40°\mathrm{C}$ from (Poxon, 2012) and $40°\mathrm{C}$ (testing in this study) were selected to fit the model parameters of the function $H(T)$. As seen in Fig. 2a, the PMI foam specimens ($100\,\mathrm{mm}\times100\,\mathrm{mm}\times50\,\mathrm{mm}$) are tested on a universal testing machine with an environmental chamber (MTS-5T, MTS, USA) according to ASTM D1621 standard with the same density $51\,\mathrm{kg/m^3}$ and loading rate $0.01\,\mathrm{s^{-1}}$ as these in (Poxon, 2012).

Figure 2b first presents the compressive stress-strain curves of the PMI foam at $-70°\mathrm{C}$, $-40°\mathrm{C}$ and $40°\mathrm{C}$ obtained from the experiment (solid lines), respectively. It shows that the PMI foam will soften (decrease in stress) with an increase of temperature, and so the elastic modulus and plateau stress will decrease accordingly. By fitting the experimental curves using function terms of $f(\varepsilon)H(T)$, parameters of $H(T)$ are obtained, that is $a = 0.016$, $b = 0.26 + 0.0016T$, and $c = 0.042$. As shown in Fig. 2b, it indicates that the fitting curves at $-70°\mathrm{C}$, $-40°\mathrm{C}$ and $40°\mathrm{C}$ are basically consistent with the experimental curves.

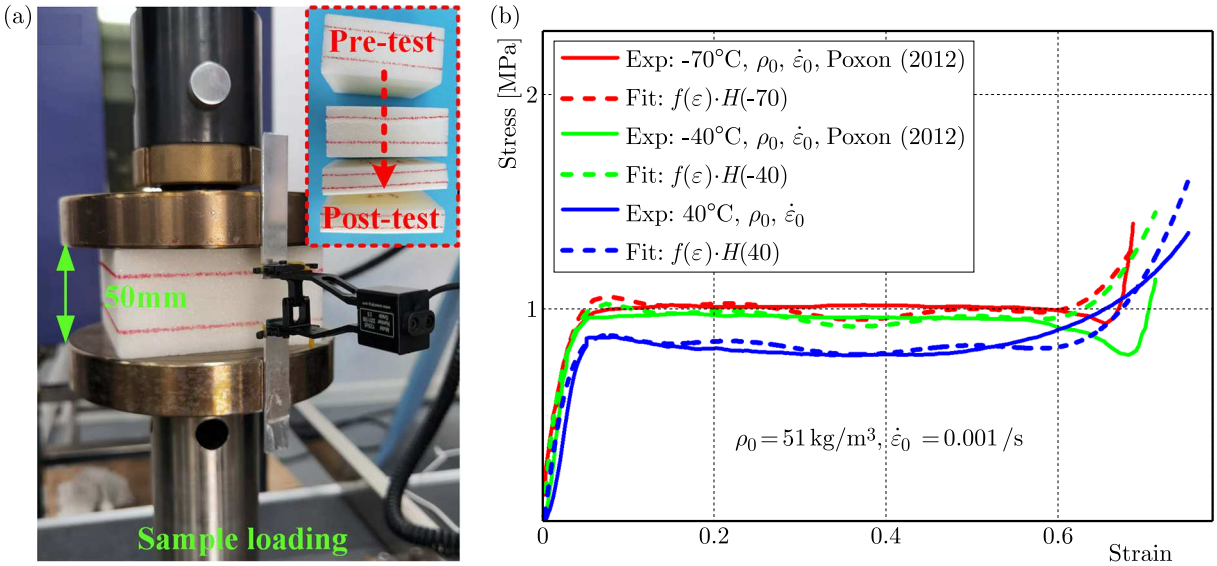

Fig. 2. (a) Compression test of the PMI foam, (b) experimental curves from testing and fitting curves with the temperature function $H(T)$

3.1.3. Determination of density function parameters

Similarly, the density of the PMI foam will also significantly affect its compressive mechanical behavior. Keeping the temperature $T_0 = 20°\mathrm{C}$ and strain rate $\dot{\varepsilon}_0 = 0.01\,\mathrm{s}^{-1}$ unchanged and only changing the density $\rho = 71$, 110 and $200\,\mathrm{kg/m^3}$, the experimental stress-strain curves (Rohacell 71WF, 110WF, 200WF) from (Poxon, 2012) are given in Figs. 3a-c, which (solid lines) exhibit that the higher the density of foam, the greater the yield stress, the shorter the yield plateau section, and the steeper the dense section. The linear function of relative density (G_1, Eq. (2.4)) and the modified Freundlich model (G_2, Eq. (2.5)), as well as the newly constructed density function (G_3, Eq. (2.6)) are used to fit the compressive stress-strain curves with different densities, and the fitted results are respectively given in Figs. 3a-c (dashed lines). Figure 3a indicates that the fitting results of the function G_1 to the stress-strain curve of a low-density PMI foam $\rho = 71$ and $110\,\mathrm{kg/m^3}$ is relatively good, but is seriously deviated for a high-density PMI foam (e.g., $200\,\mathrm{kg/m^3}$). That is, the linear function G_1 is only applicable to the low-density PMI foam. While, as shown in Figs. 3b and 3c, the G_2 and G_3 functions show highly consistent fitting results for these three densities (71, 110 and $200\,\mathrm{kg/m^3}$), respectively.

The fitting errors, $(\sigma_{fit} - \sigma_{exp})/\sigma_{exp}$, from these three density functions (G_1, G_2, G_3), are presented in Fig. 3d. It can be seen that the fitted results of the G_2 and G_3 functions show smaller errors than the G_1 function when ρ is 71 or $110\,\mathrm{kg/m^3}$ (the fitting error of the function G_1 at $\rho = 200\,\mathrm{kg/m^3}$ is too large, so the error curve is absent in Fig. 3d). In addition, Fig. 3d also indicates that the error curves obtained from the G_2 and G_3 functions basically coincide with each other when ρ is 71 or $110\,\mathrm{kg/m^3}$. Moreover, when ρ is $200\,\mathrm{kg/m^3}$, the error from the function G_3 is slightly smaller that of the function G_2. Therefore, for the function G_3 (Eq. (2.6)), the relationships between the model parameters and the relative density of the PMI foam are then fitted, as shown as

$$\begin{aligned} P(\rho^*) &= 2.68 - 1.37\rho^* + 0.37\rho^{*2} \\ Q(\rho^*) &= 0.0094 - 0.011\rho^* + 0.0031\rho^{*2} \\ R(\rho^*) &= -0.0051 + 0.032\rho^* \end{aligned} \tag{3.1}$$

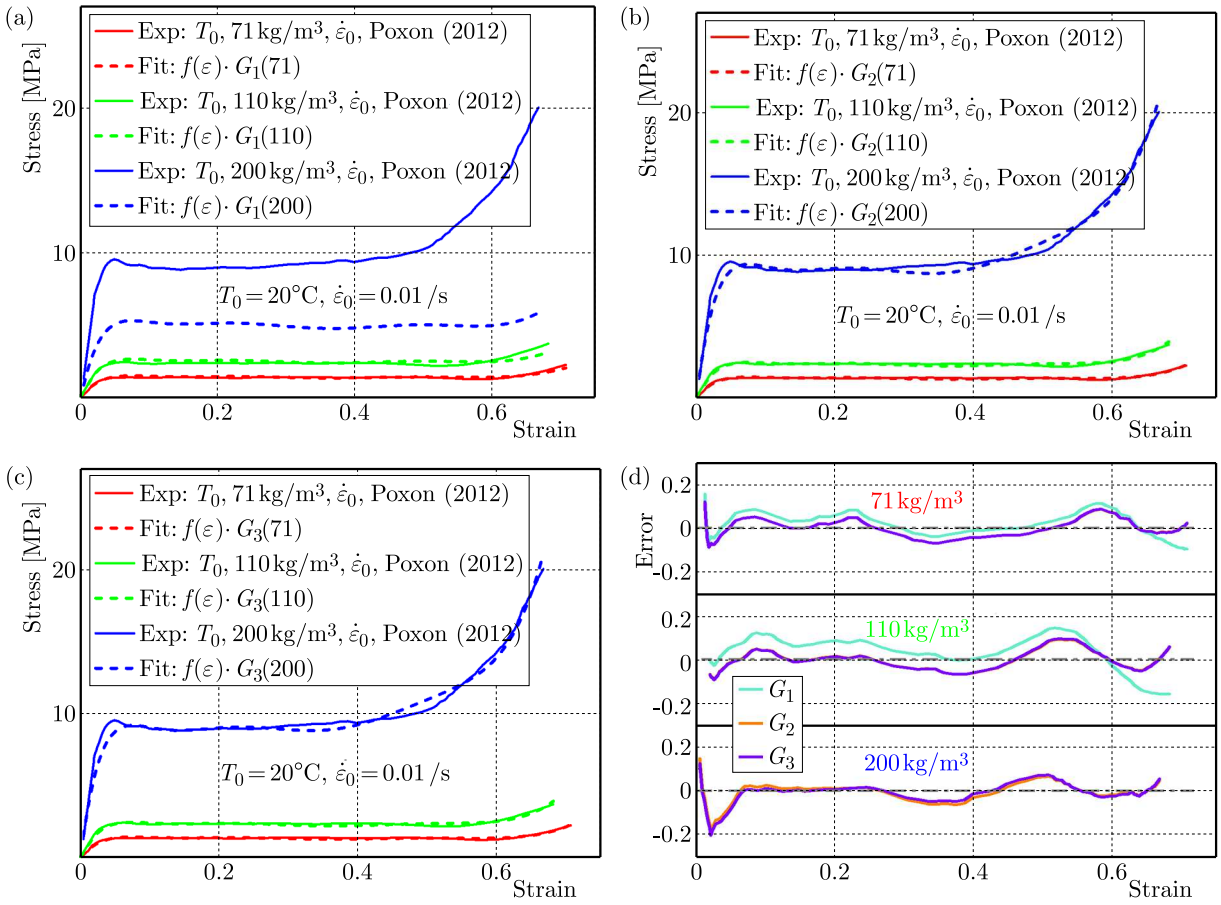

Fig. 3. Comparison between experimental curves and density function fitting curves of (a) G_1, (b) G_2 and (c) G_3, (d) comparison of fitting errors for different density functions

3.1.4. Determination of strain-rate function parameters

Subsequently, the influence of the strain rate is considered, since the compressive mechanical behavior of the PMI foam is also sensitive to it. Keeping $\rho_0 = 51\,\mathrm{kg/m^3}$ and $T_0 = 20°\mathrm{C}$ unchanged, and just changing the strain-rate ($\dot{\varepsilon} = 8.3 \cdot 10^{-4}\,\mathrm{s^{-1}}$, 9.1 and $100\,\mathrm{s^{-1}}$), the strain--rate functions, M_1 Eq. (2.7), M_2 Eq. (2.8) and M_3 Eq. (2.9) are sequentially selected to fit the experimental curves (Rohacell 51WF) obtained from (Flores-Johnson *et al.*, 2008) and (Poxon, 2012). Figures 4a-c present a comparison between the fitted curves and the experimental curves, respectively, which show that the higher the strain-rate, the greater the yield stress and the shorter the yield plateau section. Among them, Fig. 4a indicates that the Seeger model M_1 fits well with the curve when $\dot{\varepsilon} = 8.3 \cdot 10^{-4}\,\mathrm{s^{-1}}$ (quasi-static loading). However, when $\dot{\varepsilon} = 9.1$ and $100\,\mathrm{s^{-1}}$, the plateau section fitted by the function M_1 is higher, while the densification section is relatively lower. That is, the function M_1 is not suitable for high strain-rate situations. And as can be seen in Fig. 4b, M_2 also performs well under the quasi-static condition, and has improvements in the first half of the plateau section and the densification section when compared to M_1 function, but not sufficient. On the contrary, the function M_3 can fit the experimental stress-strain curves well for these three strain rates, as can be seen in Fig. 4c.

Especially, compared to M_1 or M_2, M_3 shows superior fitting accuracy in the densification section, as shown in Fig. 4d. Therefore, the relationships between the model parameters of the function M_3, Eq. (2.9), and the strain-rate are then obtained, as seen in Eqs. (3.2)

$$
\begin{aligned}
i &= 0.037 - 0.0024 \ln \frac{\dot{\varepsilon}}{\dot{\varepsilon}_0} + 6.11 \cdot 10^{-5} \Big(\ln \frac{\dot{\varepsilon}}{\dot{\varepsilon}_0} \Big)^2 \\
j &= 217.89 - 40.34 \ln \frac{\dot{\varepsilon}}{\dot{\varepsilon}_0} + 1.82 \Big(\ln \frac{\dot{\varepsilon}}{\dot{\varepsilon}_0} \Big)^2 \\
k &= 55.61 - 8.22 \ln \frac{\dot{\varepsilon}}{\dot{\varepsilon}_0} + 0.32 \Big(\ln \frac{\dot{\varepsilon}}{\dot{\varepsilon}_0} \Big)^2
\end{aligned}
\tag{3.2}
$$

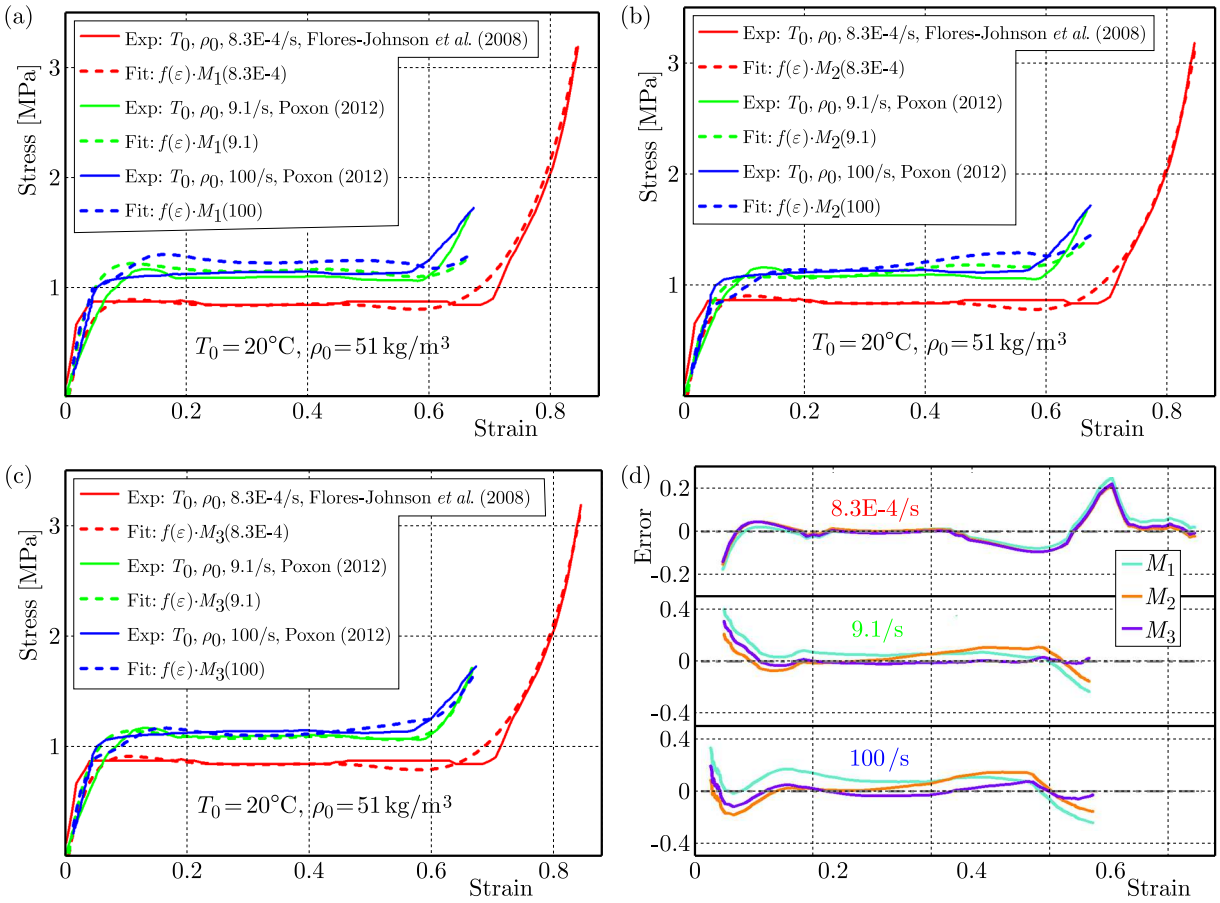

Fig. 4. Comparison between experimental curves and strain-rate function fitting curves of (a) M_1, (b) M_2 and (c) M_3, (d) comparison of fitting errors for different strain-rate functions

It can be seen from Figs. 2 and 4 that the effects of strain-rate and temperature on the compression stress-strain curve of the PMI foam are opposite, which can be simply linked through the time-temperature equivalence principle (Poxon, 2012). That is, the mechanical behavior of the PMI foam at a certain strain-rate can be mapped to the response at a certain temperature. For example, for the PMI foam, when $\rho = 51\,\mathrm{kg/m^3}$, the mechanical behavior of $T = 20°\mathrm{C}$ and $\dot{\varepsilon} = 100\,\mathrm{s^{-1}}$ can be mapped to each other, and the same is true for the mechanical behavior of $T = -70°\mathrm{C}$ and $\dot{\varepsilon} = 0.001\,\mathrm{s^{-1}}$. Also, when $\rho = 200\,\mathrm{kg/m^3}$, the state of $T = 20°\mathrm{C}$ and $\dot{\varepsilon} = 1000\,\mathrm{s^{-1}}$, and the state of $T = -70°\mathrm{C}$ and $\dot{\varepsilon} = 0.001\,\mathrm{s^{-1}}$ can be mapped to each other too, as can be referenced in the study carried by Poxon (2012).

3.2. Verification by experimental curves

The improved phenomenological constitutive model of the PMI foam based on the Sherwood-Frost model is obtained in Section 3.1, in which the effects of temperature, density and strain-rate on the compression stress-strain curves can be considered simultaneously. The stress-strain curves from case 1 ($\rho = 51\,\mathrm{kg/m^3}$, $T = 80°\mathrm{C}$, $\dot{\varepsilon} = 0.01\,\mathrm{s^{-1}}$), case 2 ($\rho = 110\,\mathrm{kg/m^3}$, $T = 20°\mathrm{C}$,

$\dot{\varepsilon} = 0.01\,\mathrm{s}^{-1}$) and case 3 ($\rho = 51\,\mathrm{kg/m^3}$, $T = 20°\mathrm{C}$, $\dot{\varepsilon} = 0.1\,\mathrm{s}^{-1}$) are obtained by compressive testing (as seen in Fig. 2a), which are used to verify the $H(T)$, G_3 and M_3 functions in the improved model. As shown in Fig. 5a-c, the experimental curves (solid lines) and the verified curves (dashed lines) are quite consistent, and the error margins are -13.39%-$+4.76\%$ (case 1), -9.94%-$+9.52\%$ (case 2), and -3.69%-$+5.41\%$ (case 3), respectively, which indicates that the modified model can effectively predict the compressive stress-strain curves of the PMI foam. Among them, in case 1, due to the temperature effect ($T = 80°\mathrm{C}$), the transition zone between the plateau and densification section is becoming less apparent, resulting in slightly higher errors compared to the other two. Moreover, compressive testing under $\rho = 51\,\mathrm{kg/m^3}$, $T = 120°\mathrm{C}$ and $\dot{\varepsilon} = 0.00167\,\mathrm{s}^{-1}$ (case 4) is also conducted to characterize the fitting effect of the model on the coupling effect of strain-rate and temperature, as shown in Fig. 5d, indicating a relatively small fitting error. However, under low strain-rates, the fitting results of the transition section from the elastic stage to the plateau section (the curve knee) are poor and further improvement is needed. At the same time, when the temperature reaches 120°C, the transition zone between the plateau and densification section is no longer obvious (Xing *et al.*, 2024), so the fitting result of this zone is also poor.

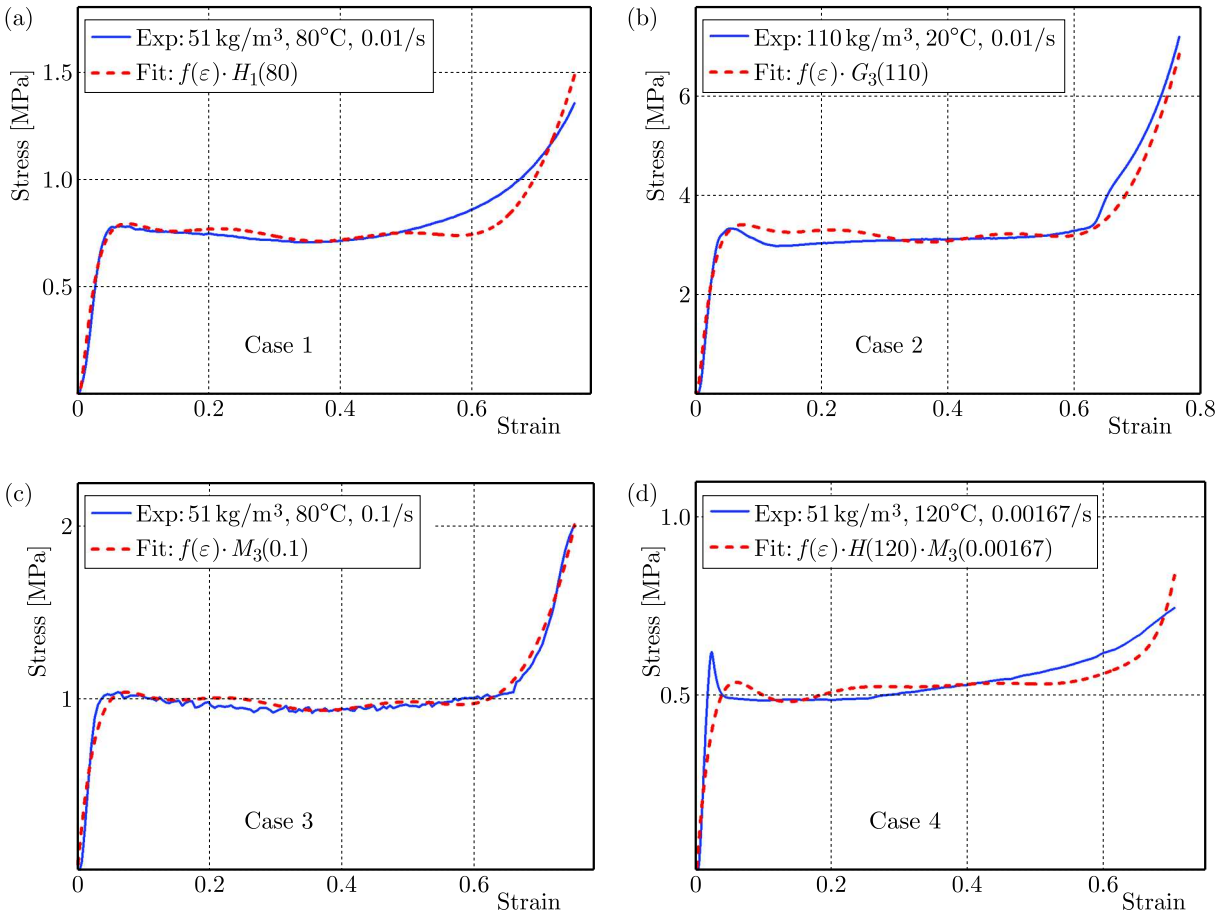

Fig. 5. Experiment and verification curves of (a) $H(T)$, (b) G_3, (c) M_3 and (d) $H(T)$ coupled with M_3

3.3. Finite element (FE) calculation verification

Abaqus software is used to model the uniaxial compressive mechanical behavior of the PMI foam (Rohacell 51WF). Figure 6a displays the FE model for compression specimens using element C3D8R, where, a simple model consists of a cuboid foam (100 mm×100 mm×50 mm, same size as specimens in Fig. 2a) and two rigid compression surfaces with boundary and loading

conditions. The PMI foam properties are input through an elastic-plastic model in the property module. In the elastic term, the foam modulus of temperature effect $T = 80°\mathrm{C}$ and strain rate effect $\dot{\varepsilon} = 0.1\,\mathrm{s}^{-1}$ are 44.68 MPa and 69.09 MPa, respectively, and the Possion ratio is 0.33. In the plastic term, 0.013 and 0.011 are respectively selected as yield strains for the temperature effect and strain rate effect, and the plastic strain and stress data generated by the improved model (Eqs. (2.2) and (2.3) with parameters are obtained in Section 3.1 for the temperature effect, as well as Eqs. (2.2), (2.9) and (3.2) for the strain rate effect) are used as the foam plastic property. The reference points coupled with the rigid surfaces are established for the purpose of applying loads and extracting the constraint reaction force, where the bottom one is constrained in all directions, while the upper one only unconstrained in the z-direction, and the foam compression process is simulated by moving it down. Moreover, universal contact (hard contact, penalty algorithm) is used between the surfaces and the foam. By conducting mesh sensitivity analysis on the model, an ideal mesh size of 2 mm is obtained.

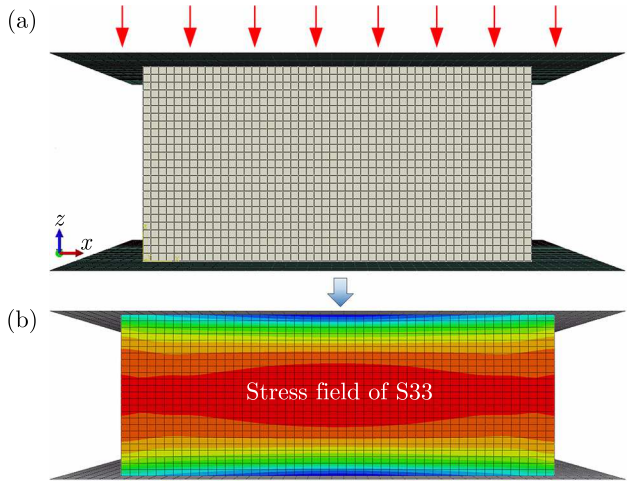

Fig. 6. Compressive simulation of the PMI foam (a) model with boundary and loading conditions, and (b) stress field of z-direction during the compression

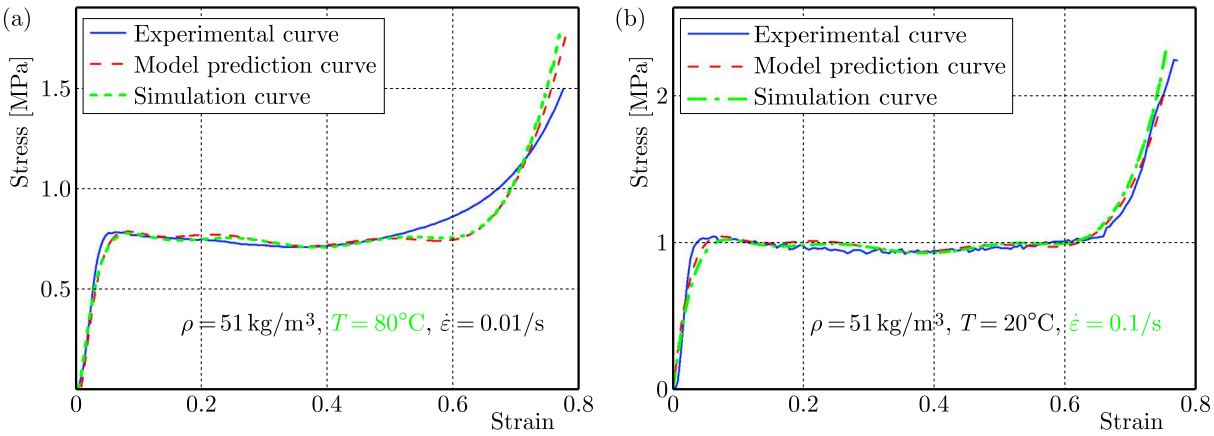

Fig. 7. Comparison curves of experimental, model prediction and simulation (a) temperature effect, (b) stress-rate effect

The simulation results show that the stress concentration first occurs in the center of the foam, as shown in Fig. 6b, which is consistent with the experimental results as given in Fig. 2a. The calculation results of temperature and strain-rate effects obtained by converting the force and displacement of the reference point are shown in Figs. 7a and 7b, respectively, which indicate a good agreement with the experimental results. Therefore, experimental and simulation

verifications prove that the improved model proposed in the present work can well predict the mechanical response of a PMI foam during uniaxial compression when the effects of density, temperature and strain rate are considered separately or simultaneously.

4. Conclusions

The constitutive model of the foam plays a decisive role in the design and failure analysis of foam sandwich structures. There are few studies on the constitutive model of the PMI foam, and often only a single variable is considered, such as density or temperature. In this work, a constitutive model for the PMI foam has been proposed to describe the compressive mechanical behavior simultaneously considering density, temperature and strain rate. Key conclusions drawn from this study are summarized here:

- Based on the traditional Sherwood-Frost constitutive model and combined with the experimental data of the PMI foam, a new improved constitutive model containing new function terms of temperature, density, and strain rate for the PMI foam is proposed.
- The parameters of the temperature term, density term and strain-rate term in the new model are successively obtained by fitting the compressive stress-strain curves under different temperatures, densities and strain-rates. The new model shows a higher accuracy when comparing with the terms proposed in the previous studies.
- The new model is well verified by the compressive experimental data (error ranges, -13.39%-$+4.76\%$ for case 1, -9.94%-$+9.52\%$ for case 2, and -3.69%-$+5.41\%$ for case 3) and numerical simulation curves at different temperatures, densities and strain-rates, which can successfully predict the compressive mechanical response of the PMI foam if the effects of temperature, density and strain-rate are concurrently considered, and the error is within an acceptable range.

Acknowledgements

The authors would like to thank for the financial support from the National Natural Science Foundation of China (No. 12272268).

References

1. Chai H.W., Xie Z.L., Xiao X.H., Xie H.L., Huang J.Y., Luo S.N., 2020, Microstructural characterization and constitutive modeling of deformation of closed-cell foams based on in situ x-ray tomography, *International Journal of Plasticity*, **131**, 102730
2. Flores-Johnson E.A., Li Q.M., Mines R.A.W., 2008, Degradation of elastic modulus of progressively crushable foams in uniaxial compression, *Journal of Cellular Plastics*, **44**, 5, 415-434
3. Hedayati R., Sadighi M., 2018, Low-velocity impact behaviour of open-cell foams, *Journal of Theoretical and Applied Mechanics*, **56**, 4, 939-949
4. Hu S., Liu J., Wang W., 1998, Study of the constitutive relationship of rigid polyurethane foam (in Chinese), *Chinese Journal of Theoretical and Applied Mechanics*, **30**, 2, 151-156
5. Huo X., Jiang Z., Luo Q., Li Q., Sun G., 2022, Mechanical characterization and numerical modeling on the yield and fracture behaviors of polymethacrylimide (PMI) foam materials, *International Journal of Mechanical Sciences*, **218**, 107033
6. Jeong K.Y., Cheon S.S., Munshi M.B., 2012, A constitutive model for polyurethane foam with strain rate sensitivity, *Journal of Mechanical Science and Technology*, **26**, 7, 2033-2038
7. Li Q.M., Mines R.A.W., Birch R.S., 2000, The crush behaviour of Rohacell-51WF structural foam, *International Journal of Solids and Structures*, **37**, 43, 6321-6341

8. Li X.Q., Tao J.L., Landauer A.K., Franck C., Henann D.L., 2022, Large-deformation constitutive modeling of viscoelastic foams: Application to a closed-cell foam material, *Journal of the Mechanics and Physics of Solids*, **161**, 104807
9. Maier L., Hu P., Seibert H.F., 2006, PMI foam cored sandwich components produced by means of different manufacturing methods (in Chinese), *Journal of Materials Engineering*, 5, 37-40, 45
10. Meinecke E.A., Schwaber D.M., 1970, Energy absorption in polymeric foams. I. Prediction of impact behavior from Instron data for foams with rate-independent modulus, *Journal of Applied Polymer Science*, **14**, 9, 2239-2248
11. Palamidi E., 2010, Hopkinson bar testing of cellular materials, Ph.D. Thesis, University of Manchester, Manchester
12. Poxon S., 2012, The mechanical response of low to high density Rohacell foams, Ph.D. Thesis, University of Oxford, Oxford
13. Rahimidehgolan F., Altenhof W., 2023, Compressive behavior and deformation mechanisms of rigid polymeric foams: A review, *Composites Part B: Engineering*, **253**, 110513
14. Rusch K.C., 1969, Load-compression behavior of flexible foams, *Journal of Applied Polymer Science*, **13**, 11, 2297-2311
15. Seibert H.F., 2006, Applications for PMI foams in aerospace sandwich structures, *Reinforced Plastics*, **50**, 1, 44-48
16. Sherwood J.A., Frost C.C., 1992, Constitutive modeling and simulation of energy absorbing polyurethane foam under impact loading, *Polymer Engineering and Science*, **32**, 16, 1138-1146
17. Xing Z., Cen Q., Wang Q., Li L., Wang Z., Liu L., 2024, Compressive mechanical behavior and corresponding failure mechanism of polymethacrylimide foam induced by thermo-mechanical coupling, *Polymers*, **16**, 9, 1199

Manuscript received July 21, 2024; accepted for publication November 11, 2024